geosciences

Article

Microfacies and Stratigraphic Observations from the Bulz Dolomite Formation (Apuseni Mountains, Romania): Implications for Paleoenvironment and Regional Correlation

Béla Raucsik [1,*,†], Andrea Varga [1,†], Olga Piros [2], Andrea Szuromi Korecz [3] and Elemér Pál-Molnár [1]

[1] Department of Geology, University of Szeged, 6722 Szeged, Hungary; raucsikne.varga.andrea.beata@szte.hu (A.V.); pal-molnar.elemer@szte.hu (E.P.-M.)
[2] Hungarian Geological Society, 1015 Budapest, Hungary; pirosolga1@gmail.com
[3] Independent Researcher, 1194 Budapest, Hungary; kaszuroka@ttk.elte.hu
* Correspondence: raucsik.bela@szte.hu
† These authors have contributed equally to this work.

Abstract

The Middle Triassic Bulz Dolomite Formation in the Apuseni Mountains (Romania) lacks detailed microfacies documentation and paleoenvironmental reconstruction, leaving its regional correlation unresolved. This study aims to describe the microfacies and fossil assemblages of the Bulz Dolomite to reconstruct the Anisian depositional environment and establish regional stratigraphic links. More than twenty outcrop samples were analyzed using conventional microfacies analysis, UV/VIS-fluorescence, and cathodoluminescence microscopy. Results reveal that early, fabric-retentive dolomitization preserved microbial boundstones, dasycladalean algae (*Teutloporella peniculiformis*, *Physoporella pauciforata*), and benthic foraminifers (*Hoyenella sinensis*), indicating shallow-marine, peritidal, and restricted lagoonal environments. The multiphase diagenetic history involves early reflux dolomitization from hypersaline brines, burial recrystallization forming nonplanar and saddle dolomites, and late-stage meteoric calcite cementation. The diagnostic fossil assemblage firmly constrains the formation to the Anisian age. Consequently, the Bulz Dolomite shares compelling lithological, diagenetic, and biostratigraphic affinities with the Szeged Dolomite Formation in the basement of the southeastern Pannonian Basin, demonstrating the presence of a unified, expansive evaporitic carbonate shelf extending across the Tisza Megaunit along the Neotethyan passive margin.

Keywords: paleoenvironment; dolomitization; microfacies; algae; foraminifers; Anisian; Apuseni Mountains; Codru nappe system

Academic Editor: Xiumian Hu

Received: 20 March 2026
Revised: 20 April 2026
Accepted: 21 April 2026
Published: 23 April 2026

1. Introduction

The Apuseni Mountains, Romania (Figure 1) have been investigated for decades, and the most relevant information about their geological evolution, stratigraphy, and correlation was summarized in several handbooks and review papers (see, e.g., [1–7]). Historical data on Triassic geology, however, are mainly restricted to explanatory notes for geological maps written in Romanian (see, e.g., [8–10]), conference guidebooks [11,12], and comprehensive summaries [6,13]. Case studies dedicated to Triassic sedimentary sequences in the Apuseni Mountains are relatively rare in the international literature [14–16].

 https://doi.org/10.3390/geosciences16050170

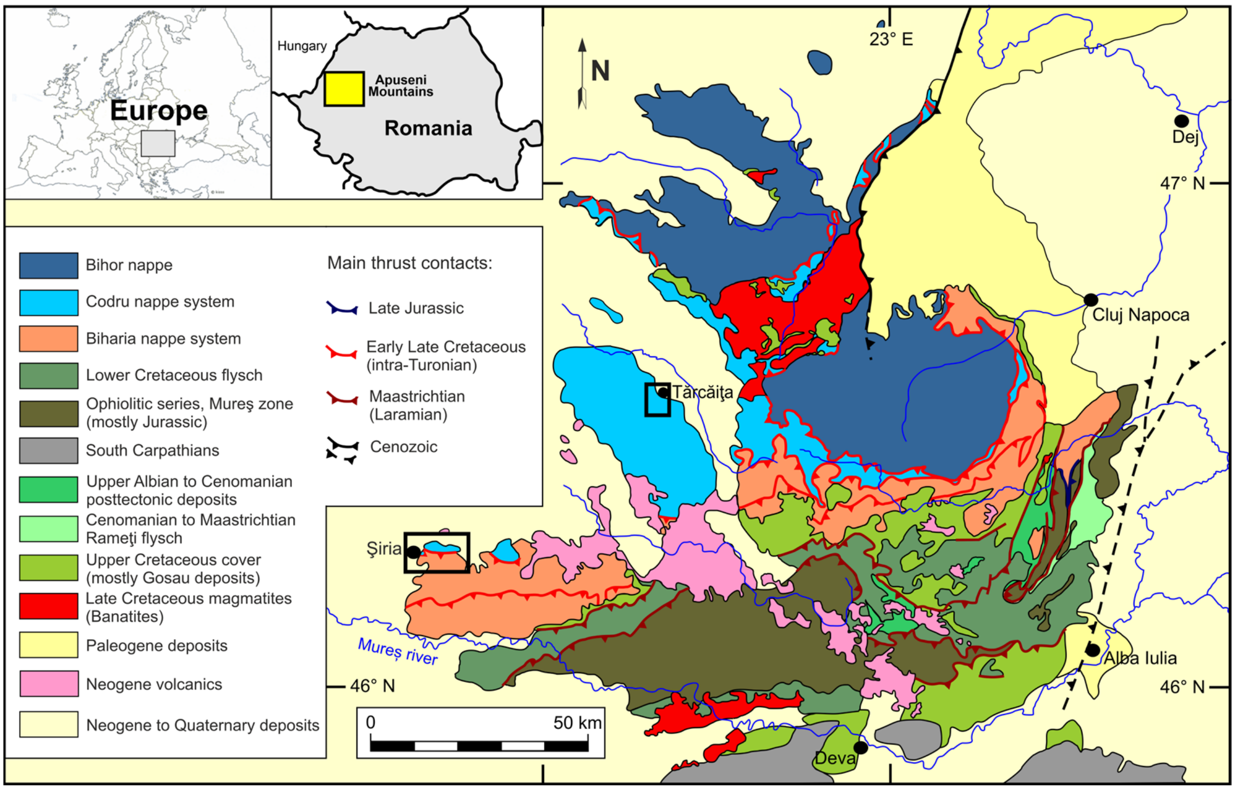

Figure 1. Geological and structural map of the Apuseni Mountains, Romania (modified after [17], and [18]), showing the study areas (black rectangles). Inset sketch maps show the position of the Apuseni Mountains in Europe.

West of the Apuseni Mountains, in the southeastern part of the pre-Neogene basement of the Pannonian Basin, a dolomitized Middle Triassic (Upper Anisian–Ladinian) carbonate sequence (Szeged Dolomite Formation, Szeged Basin, Hungary) is known, which is an intensively explored hydrocarbon reservoir [19,20]. According to Bleahu et al. [3], the Szeged Dolomite is regarded as a basement equivalent of the Anisian Bulz Dolomite of the Apuseni Mountains. However, the correlation between these formations has not been resolved by microfacies and stratigraphic data in a satisfactory manner.

Dolomite-forming processes commonly destroy the sedimentary features and characteristics of the precursor carbonates. Therefore, dolomite rocks usually neither preserve the textures of the original limestone nor the fossils therein (see, e.g., [21–23]). In the Triassic succession of the Szeged Basin, hydrocarbon exploration studies [19,20,24–26] revealed that the carbonate deposits were generally subjected to pervasive dolomitization and recrystallization. Locally, however, the Szeged Dolomite Formation was only affected by partial dolomitization or remained undolomitized. Based on a well-preserved and exceptionally rich fossil assemblage [27], including a *Hoyenella*–*Glomospirella*–*Glomospira*-dominated foraminifer assemblage, algal colonies, ostracods, gastropods, and bivalve shells. Backreef–lagoon environments and seawaters of elevated salinity have been proposed for the time of deposition.

Based on current knowledge, fossils are generally uncommon in the Bulz Dolomite [11,12], although relatively well-preserved fauna is occasionally observed. At the microscale, fossils and other characteristic grains can remain as faint shadows outlining their original shapes and occasionally preserving internal details. Despite its regional importance, the detailed microfacies features of the Bulz Dolomite Formation remain practically undocumented in the international literature. To bridge this knowledge gap, this study provides the first comprehensive microfacies and micropaleontological documentation of dolomite samples collected from the most promising outcrops of the Anisian Bulz Dolomite in the Highiş Mountains near Şiria and the Codru–Moma Mountains near Tărcăiţa (Figure 1). Furthermore, by establishing the foundational diagenetic framework of the Bulz Dolomite and systematically comparing its depositional settings and diagenetic features with those of the Szeged Dolomite Formation, we offer novel, petrographic evidence to support their long-standing but poorly documented correlation. Synthesizing these new data with published paleoenvironmental models, this research significantly advances the paleogeographic reconstruction of the Anisian carbonate ramp. While the exhaustive geochemical modeling of the diagenetic history (involving fabric-selective stable isotope and trace element measurements) is currently in progress, the comparative microfacies and diagenetic findings presented here redefine our understanding of these regionally crucial formations.

Geological Background

The Apuseni Mountains (hereafter AM) are located at the eastern rim of the Pannonian Basin, in western Romania (Figure 1). They have been subdivided into four tectonostratigraphic units, including the Bihor nappe (or autochthon/parautochthon unit), Codru nappe system (hereafter Codru NS), Biharia nappe system, and Mureş zone unit [17,28]. The investigated areas comprise different parts of the Codru NS within the Tisza megaunit [3,17], where the Mesozoic succession, including Triassic formations (Figure 2), is exposed at the surface. The Codru NS consists of N–NW-vergent cover nappes such as the Finiş, Dieva, and Moma nappes, mostly detached from their original basement [3,12].

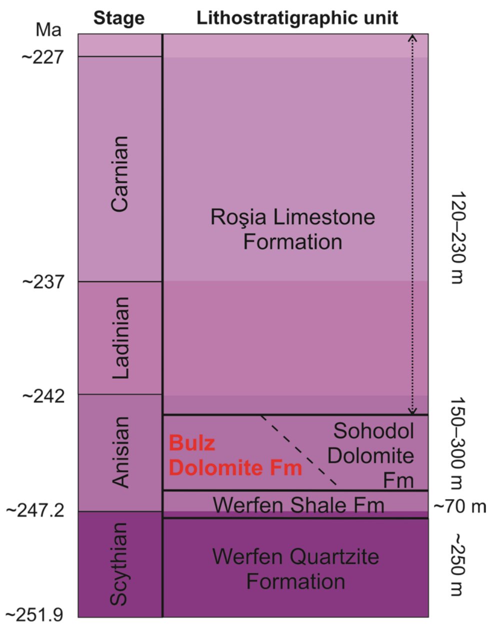

Figure 2. Schematic stratigraphic column of the Triassic succession of the AM [12], highlighting the Anisian Bulz Dolomite Formation, Finiş nappe of the Codru NS. The total thickness of the lithostratigraphic units, according to Bleahu et al. [3], is also indicated. Notes: Norian and Rhaetian formations are not included; stratigraphic range of Roşia Limestone Formation is indicated by double-headed arrow. Fm = Formation.

During the Triassic period, different depositional units of the Codru NS were situated on the European shelf of the Neotethys, corresponding to shelf margin settings [3,4]. The Lower Triassic continental (fluvial and deltaic) deposits are mainly represented by red siliciclastic rocks (Werfen Quartzite Formation [12]). As a result of a relative sea-level rise, the depositional environment evolved into a vast carbonate ramp system during the Early and Middle Anisian. The lowermost Anisian pelitic sequence (known as "Werfen Shales") is the first marine succession deposited in a coastal plain and sabkha environment. In the Codru NS, especially in the Finiş nappe, Patrulius et al. [12] distinguished two heteropic types of Anisian dolomites (Figure 2). (i) Thick-bedded, gray, coarse-crystalline, massive dolomites (known as the Sohodol Dolomite Formation) represent depositional environments in periodically emergent shoals. (ii) Medium- to thin-bedded, dark gray to black, fine-crystalline dolomites with some pelitic and limestone intercalations (known as the Bulz Dolomite Formation) were formed in lagoons with restricted oxygenation. The Anisian rifting stage caused the disintegration of the ramp system that was differentiated into Reifling-type intrashelf basins and shallow-water Wetterstein-type reef–lagoon complexes. According to the interpretation of [3], the platform facies were limited to narrow zones between the extended basins. Characteristic basinal sediment in most of the Codru NS is the Roşia Limestone Formation, which conformly overlies the Anisian dolomites (Figure 2).

The present study investigates the Bulz Dolomite Formation, which occurs in the Codru–Moma Mountains (the Dieva and Moma nappes) and the northwestern rim of the Highiş Mountains (the southern part of the Finiş nappe [12]). In the Highiş Mountains, the Bulz Dolomite represents the youngest Mesozoic formation [8]. Generally, the fossil record of the Anisian dolomites is poor, but small gastropods, bivalves (*Costatoria costata*: Galşa, Highiş Mountains; *Lyriomyophoria elegans*: Codru–Moma Mountains), and crinoids (*Dadocrinus*: upper part of the Moma nappe) have been reported from some localities [11,12].

2. Materials and Methods

In the Highiş Mountains near Şiria, two locations were chosen to sample the Bulz Dolomite (Figure 3a): (1) The Galşa section (location ID: G1; coordinates: N 46.27526, E 21.67953) exposes thin-bedded, dark to light gray, very fine- to very coarse-crystalline dolomite rocks. (2) The Măderat quarry (location ID: MDK; coordinates: N 46.27592, E 21.68548) comprises thick-bedded, light to dark gray, massive dolomites, which are typically very fine- to medium-crystalline. In the Codru–Moma Mountains near Tărcăiţa (Figure 3b), sampling site Valea cea Mică #4 ('Little valley' #4, location ID: TKV4; coordinates: N 46.5802, E 22.3171) contains gray to brownish-gray, very fine- to fine-crystalline dolomite associated with tectonic breccia.

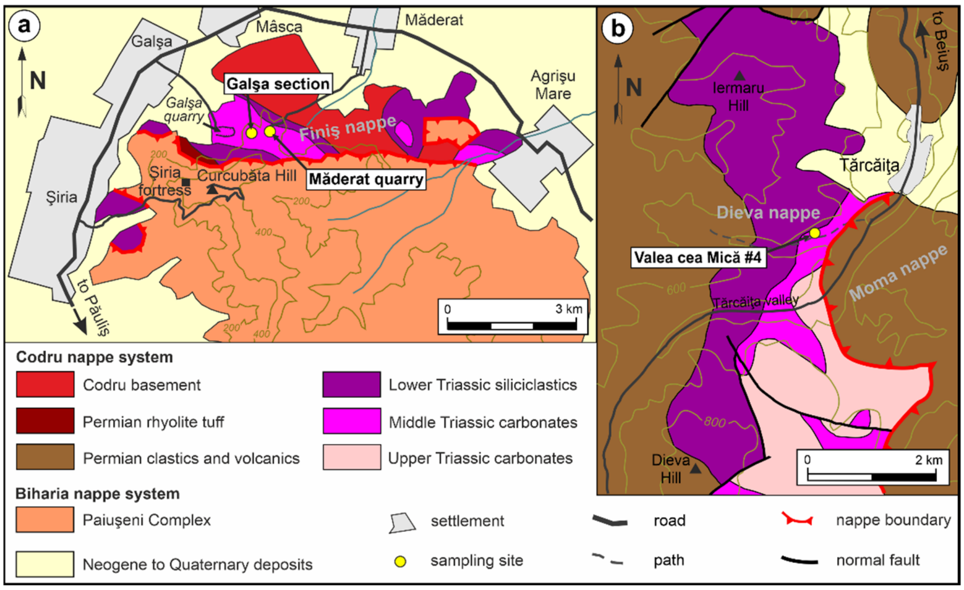

Figure 3. Geological map of the study areas in the Apuseni Mountains, Romania (based on Papiu and Ghenea [8]), showing the sampling sites (compare with the black rectangles in Figure 1). (**a**) Two sampling locations for the Bulz Dolomite in the northwestern part of the Highiș Mountains, between Şiria and Agrişu Mare. (**b**) Natural outcrop near Tărcăiţa in the Codru–Moma Mountains.

A total of more than 20 fresh samples were collected from the outcrops, representing various lithotypes such as mottled dolomite, fabric-retentive dolomite, recrystallized dolomite and dolomite breccia (Figure 4). Several specimens exhibit varying degrees of brittle deformation, characterized by hairline fractures cemented by white sparry dolomite and/or calcite crystals. Tectonic breccias are also present. Petrographic studies were performed at the Department of Geology of the University of Szeged, Hungary. To identify carbonate mineralogy (calcite, dolomite, and ferroan variants), the staining method of Dickson [29] was applied using a solution of Alizarin Red S and potassium ferricyanide.

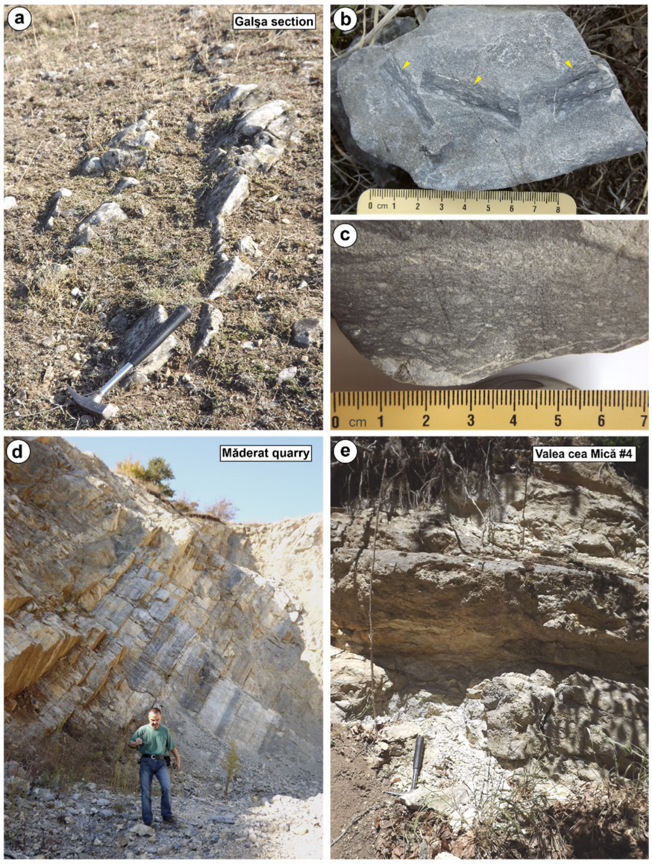

Figure 4. (**a**) Field view of thin-bedded dark gray dolomites, Galşa section. Hammer for scale is 32 cm. (**b**) Very fine- to coarse-crystalline dolomite with stromatolite rip-up clasts (arrows) showing well-preserved original limestone fabrics (sample G1.5_18). (**c**) Mottled dolomite with light gray bioclasts (green algae fragments; sample G1.5_19). (**d**) Thick-bedded dolomite succession of the Bulz Dolomite in the Măderat quarry, beds dipping 63 degrees to the south (96/63 SSW, in the convention strike, dip, dip direction). The person for scale is 1.68 m high. (**e**) Field view of strongly fractured dolomites showing slightly friable character, sampling site Valea cea Mică #4. Hammer for scale is 32 cm.

Micropetrography was conducted on ~40-μm-thick thin sections. A total of 31 thin sections (21 for G1, 6 for MDK, and 4 for TKV4 locations) were examined using an Olympus BX-41 petrographic microscope (Tokyo, Japan) equipped with a high-pressure Hg lamp and filter sets for blue–violet (400–440 nm) and ultraviolet (360–370 nm) excitation for conventional petrographic and fluorescence microscopic observations. Based on their textures, samples were selected for cathodoluminescence (CL) microscopy. Polished thin sections were analyzed with a Reliotron VII cold-cathode CL device (Bedford, MA, USA) mounted on an Olympus BX43 microscope (Tokyo, Japan), under operating conditions of 7 keV and 0.7 mA. Photomicrographs were acquired using an Olympus DP73 digital microscope camera (Tokyo, Japan).

Dolomite textures, crystal size categories, and the original microfacies, where possible, were identified in accordance with the classification scheme of Machel [21], Folk [30], and Dunham [31] with modifications by Embry and Klovan [32], respectively. The nongenetic classification of breccias by Woodcok and Mort [33] was used to describe brecciated samples.

3. Results

3.1. Galşa Section

In the Galşa section, both fabric-retentive and fabric-destructive dolomite types were identified based on microtextures (Figures 5 and 6). The degree of fabric preservation ranges from very good to complete destruction. Original sedimentary fabrics are typically better preserved in fine-crystalline dolomites. Recognizable microfacies include microbial boundstones (stromatolites), peloidal packstones or grainstones, and peloidal–bioclastic packstones, wackestones, or grainstones. The grains are mainly peloids, bioclasts (green algae fragments, ostracods, bivalve shells, crinoids, and foraminifers; Figure 5), and rare intraclasts. The dasycladalean algal assemblage includes fragments of *Teutloporella peniculiformis* Ott, *Physoporella pauciforata undulata* Bystrický, and *Physoporella pauciforata pauciforata* Bystrický (Figure 5a–d).

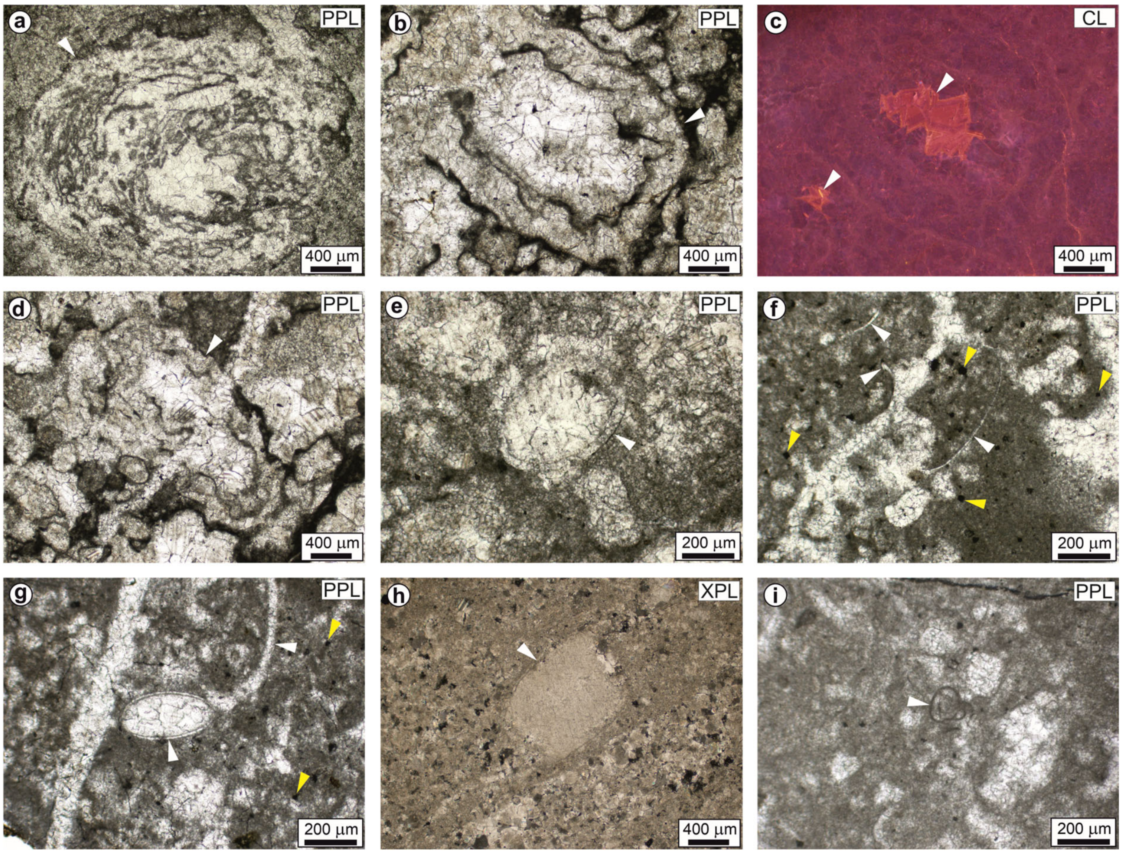

Figure 5. Bioclasts in fabric-retentive dolomite, Galşa section. (**a**) *Teutloporella peniculiformis* Ott, Dasycladaleae (sample G1.4_19). (**b**) *Physoporella pauciforata pauciforata* Bystrický, Dasycladaleae (sample G1.5_19). (**c**) Same field of view as (**b**) under CL. The matrix dolomite is very dull (lilac/pale violet) to nonluminescent. Dolomite cement (arrowed) displays red to orange concentric CL zonation. (**d**) *Physoporella pauciforata undulata* Bystrický, Dasycladaleae (arrowed, sample G1.5_19). (**e**) Poorly preserved ostracod in a very fine- to medium-crystalline matrix (arrowed, sample G1.1_19). (**f**,**g**) Very fine- to medium-crystalline dolomite with relatively well-preserved peloidal–bioclastic wackestone or packstone fabric (sample G1.E.M_18). Bioclasts were likely ostracod and bivalve shells (white arrows). Pyrite crystals are marked by yellow arrows. (**h**) Dolomitized echinoderm fragment (arrowed, sample G1.2_18). (**i**) Micritic outline of a benthic foraminifer (arrowed, sample G1.E.M_18). CL = cathodoluminescence image, PPL = plane-polarized light, XPL = crossed polars.

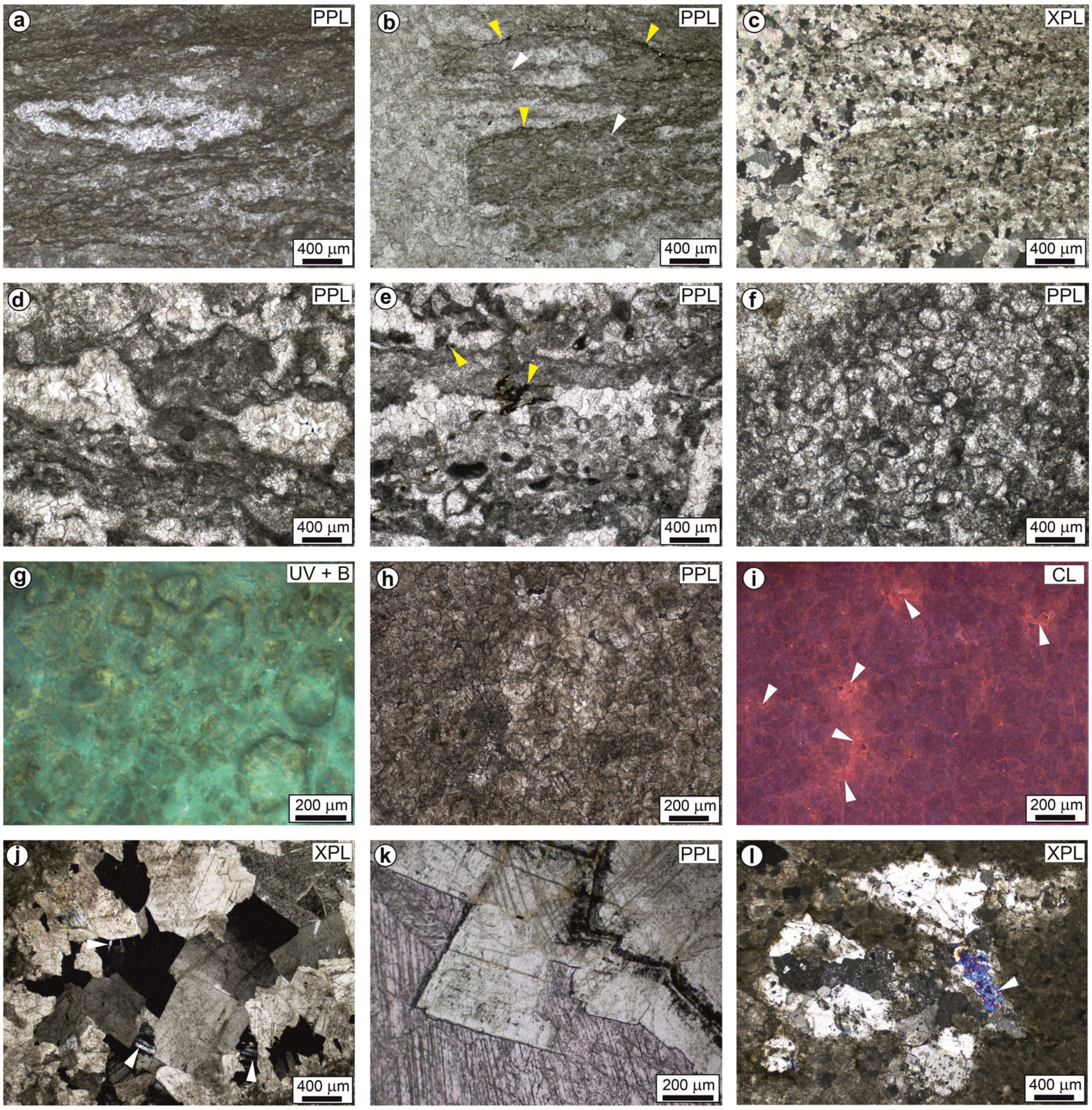

Figure 6. Fabric-retentive and fabric-destructive dolomite types, Galşa section. (**a**) Well-preserved microbial fabric in stromatolitic dolomite (sample G1.5_18). (**b**,**c**) Rip-up clast showing former microbial boundstone microfacies in fine- to coarse-crystalline dolomite (sample G1.5_18). Microstylolites (yellow arrows) are marked by brownish goethitic material. They are cross-cut by a thin fracture filled with dolomite cement (white arrows). (**d**) Perfectly preserved fenestral laminated microbialite fabric (sample G1.1_19). (**e**) Well-preserved peloidal fabric including intraclast grains (sample G1.1_19). Goethitized pyrite crystals are marked by yellow arrows. (**f**) Peloidal dolomite composed of very fine- to medium-crystalline dolomite with excellent fabric preservation (sample G1.3_19). (**g**) Ghosts of spheroidal particles suggesting a former peloidal packstone/grainstone fabric (sample G1.2_19). (**h**) Replacive dolomite crystal mosaic showing nonplanar-a to planar-s textures (sample G1.2_19). (**i**) Same field of view as (**h**) under CL. Matrix dolomite is very dull to nonluminescent. Dolomite cement (arrowed) displays red to orange CL. (**j**) Saddle dolomite cement filling a vug and exhibiting undulose extinction (sample G1.E.M_18). Deformation twins are indicated by arrows. (**k**) Coarse-crystalline dolomite rim overgrowth with a layer rich in solid inclusions arranged along planar growth zones. Late calcite cement appears pink after staining (sample G1.E.Mf_18). (**l**) Relic anhydrite (arrowed) partly replaced by late calcite (sample G1.4Bp_18). CL = cathodoluminescence image, PPL = plane-polarized light, UV + B = ultraviolet and blue–violet excitation, XPL = crossed polars.

In stromatolitic dolomite samples, the microbialite texture is perfectly preserved. Slightly undulating aphanocrystalline to fine-crystalline, nonplanar-a to planar-s dolomite laminae with irregular fenestral pores are visible (Figure 6a–d). The fenestral voids are lined with fine- to medium-crystalline, inclusion-rich dolomite. The central parts of the cavities are occluded by fine- to medium-crystalline, nonplanar-a to planar-s, limpid dolomite. Pore-filling dolomite crystals typically become coarser toward the pore center and exhibit deformation twinning. Under CL, both the nonplanar-a and planar-s matrix dolomite appear very dull (lilac/pale violet) to nonluminescent. Thin dissolution seams and sharply defined microstylolites are common and marked by brownish goethitic material.

Peloidal and/or bioclastic dolomite is composed of very fine- to coarse-crystalline, nonplanar-a to planar-s dolomite (Figure 6e,f). The crystal size distribution is typically polymodal, with finer crystals being generally turbid due to inclusions, whereas coarser crystals are limpid with occasional saddle dolomite textures, showing slightly curved crystal faces and sweeping extinction. Medium- to coarse-crystalline dolomite crystals exhibit deformation twinning. Under CL, the fabric-retentive matrix dolomite is typically very dull to nonluminescent with no zonation (Figure 5c). Coarse and saddle-like crystals, however, exhibit very weak luminescence zonation. Pyrite also appears as scattered euhedral crystals.

Fine- to medium-crystalline dolomite with poorly preserved fabric shows ghosts of peloids and/or bioclasts, or micrite envelopes that outline original grains. This tight dolomite displays slight yellowish-green fluorescence with a crystal size-dependent intensity (Figure 6g). Replacive, fabric-destructive dolomite typically shows a tight, mosaic texture composed of fine- to coarse-crystalline, planar-s dolomite crystals, which are cloudy or have cloudy cores and clear rims (Figure 6h). They have a mottled or blotchy, very dull lilac CL or appear nonluminescent (Figure 6i). The larger biomolds and vugs are filled (replaced?) by medium- to very coarse-crystalline, planar-s dolomite cement with a drusy habit. They exhibit deformation twinning and show red to orange luminescence (Figures 5c and 6i). The cement crystals in the form of rim overgrowth commonly have curved crystal cleavage and faces and show undulose extinction under crossed polars (saddle dolomite; Figure 6j). Saddle dolomite crystals exhibit marked zonation defined by alternating dark red–orange and bright red–orange bands. The final pore-occluding phase is commonly blocky calcite (Figure 6k), showing a well-developed bright yellow CL. These cement phases also occur in fracture pores.

Subordinately, nodule-like structures (up to 4 mm) are replaced by planar-s to planar-e dolomite exhibiting cloudy cores and clear rims and are filled by saddle dolomite and late calcite cement associated with goethitized pyrite crystals. In exceptional cases, this late calcite contains relics of anhydrite (Figure 6l).

3.2. Măderat Quarry

In the Măderat quarry, fabric-destructive dolomite is dominant, but subordinate fabric-retentive dolomite has also been identified with preserved peloidal–bioclastic (benthic foraminifers) wackestone, packstone or grainstone microfacies (Figure 7). The replacive dolomite is characterized by polymodal, closely packed, aphanocrystalline to fine-crystalline, nonplanar-a to planar-s texture. The degree of fabric preservation varies from moderate to none. The nature of precursor grains is typically recognizable based on micrite envelopes or inclusions that form ghosts. However, foraminifers are relatively well-preserved and are mimically replaced by aphanocrystalline to very fine-crystalline dolomite. In the foraminifer assemblage, *Hoyenella sinensis* (Ho), *Glomospira articulosa* Plummer, *Glomospira gordialis* (Jones et Parker), *Glomospira* sp., cf. *Ammodiscus* sp., and cf. *Glomospirella* sp. were observed (Figure 7a–e). Additionally, pyrite appears as scattered euhedral crystals (up to 90 µm) in the samples.

Under CL, the replacive matrix dolomite is dull red or nonluminescent (Figure 7f). They are crosscut by at least two generations of thin fractures filled with very fine- to medium-crystalline dolomite cement. The very fine-crystalline dolomite cements display red luminescence, while the coarse-crystalline ones show a brighter orange, mottled CL pattern.

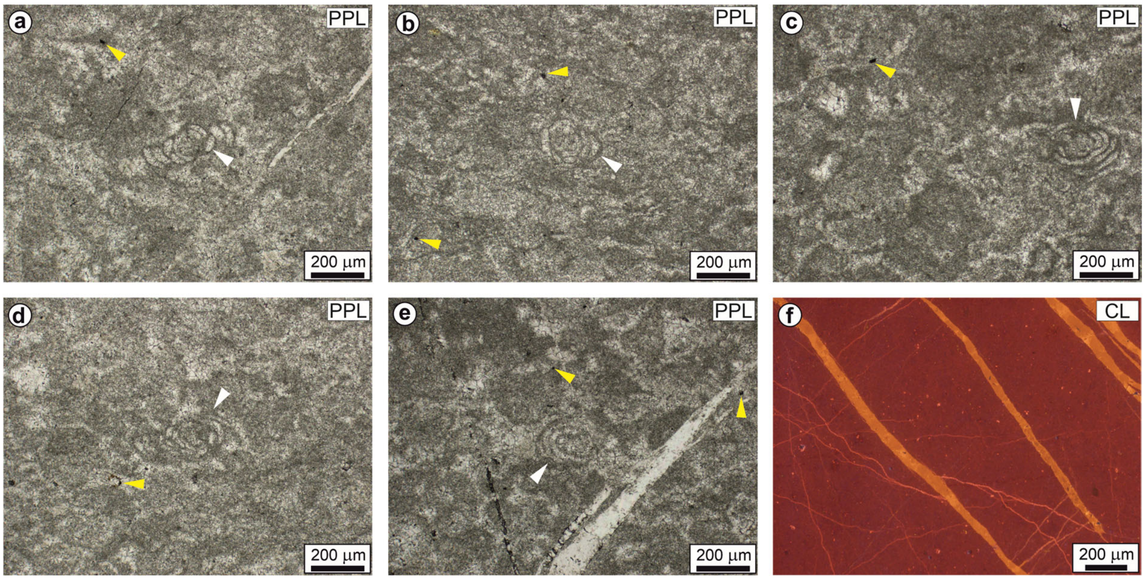

Figure 7. Micropetrographic features of the aphanocrystalline to fine-crystalline dolomite, Măderat quarry. Typically, only ghosts of globular grains are visible in the polymodal dolomite. Mimically replaced benthic foraminifers (sample MDK.3A) are indicated by white arrows. Pyrite crystals are marked by yellow arrows. (**a**) *Hoyenella sinensis* (Ho). (**b**) *Glomospira articulosa* Plummer. (**c**) *Glomospira gordialis* (Jones et Parker). (**d**) cf. *Glomospirella* sp. (**e**) cf. *Ammodiscus* sp. The very fine-crystalline ghosts suggest a peloidal grainstone or packstone precursor. (**f**) Two fracture generations are distinguished in the replacive dolomite (sample MDK.3). The older fractures are filled with very fine-crystalline dolomite cement displaying red CL, whereas the younger (and wider) fractures that crosscut the former ones are filled with fine- to medium-crystalline dolomite cement exhibiting a mottled orange CL. CL = cathodoluminescence image, PPL = plane-polarized light.

3.3. *Valea cea Mică #4 near Tărcăiţa*

At location TKV4, characterized by poor outcrop conditions, dolomite beds occur as irregular bodies (tens of cm to a few m in size) near strongly fractured zones and are largely brecciated. All of the studied rock specimens were classified as crackle breccia. Breccia clasts are minimally rotated with respect to each other and are separated by hairline cracks, reopened microstylolites, or thin seams of cement (dolomite and/or calcite).

The millimeter-to-centimeter-sized, unrounded clasts consist of fabric-retentive dolomite with a poorly to moderately preserved sedimentary texture (lithoclastic–bioclastic–peloidal packstone or grainstone) (Figure 8). In the closely packed, aphanocrystalline to fine-crystalline, nonplanar-a to planar-s dolomite, foraminifers and fragments of thin-shelled bivalves and ostracods are recognizable. In the foraminifer assemblage, *Hoyenella sinensis* (Ho), *Hoyenella* sp., and *Glomospirella* sp. were observed (Figure 8a–e). In intercrystalline pores, goethitized pyrite appears as scattered euhedral crystals and aggregates (up to 100 µm; Figure 8g). Pyrite and amorphous opaque materials also appear within microstylolites and hairline fracture porosity (Figure 8b,c).

Relatively thin fractures are present in each sample and connect irregularly shaped cavities that are lined by fine-crystalline, planar-s to planar-e dolomite. Calcite, as a second generation of cement, occurs as a fracture- and vug pore-filling mineral that is stained pink to turquoise, indicating Fe content (Figure 8h). Under CL, the aphanocrystalline to fine-crystalline matrix dolomite is dull red or nonluminescent (Figure 8i). The planar-s to planar-e dolomite cement crystals exhibit red luminescence, while the blocky calcite cement shows a well-developed orange concentrically zoned CL pattern.

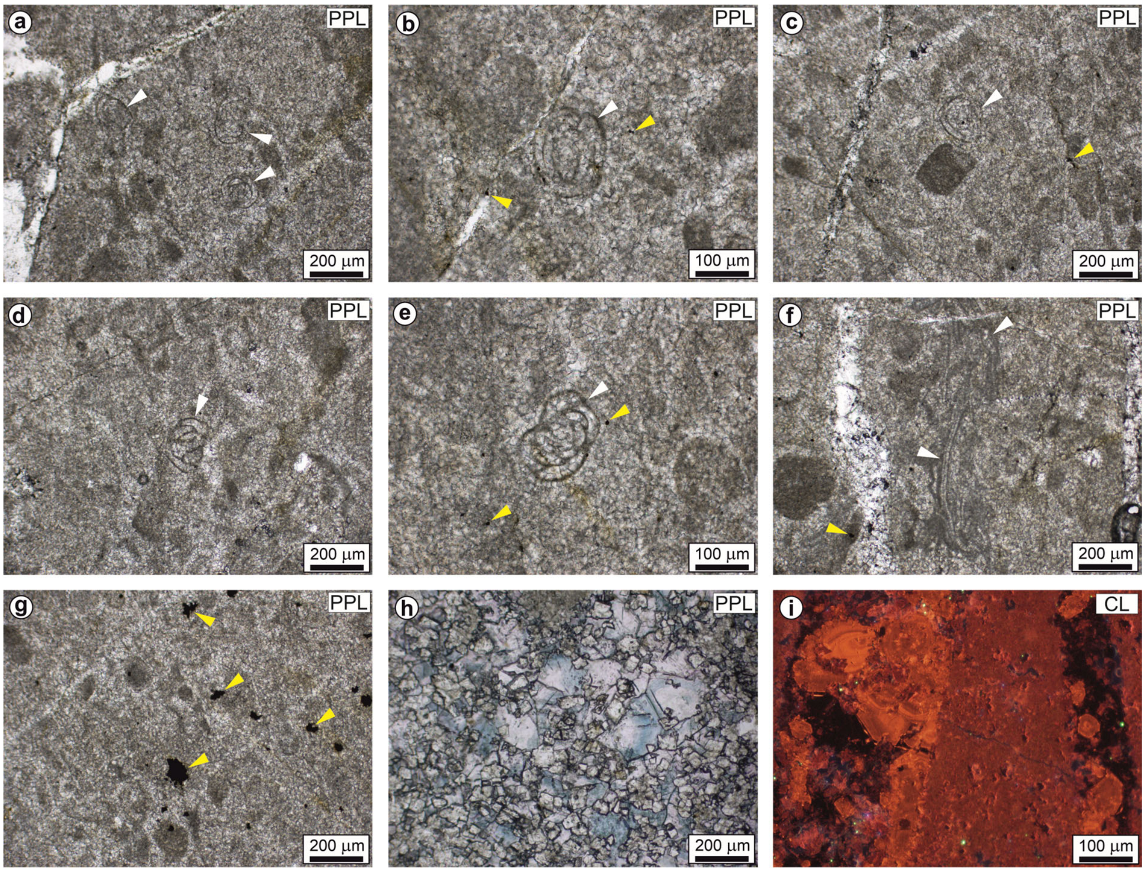

Figure 8. Micropetrographic features of the aphanocrystalline to fine-crystalline dolomite at location Valea cea Mică #4. Bioclasts are indicated by white arrows. Pyrite crystals and aggregates are marked by yellow arrows. (**a**,**b**) *Hoyenella sinensis* (Ho) (sample TKV4.1). (**c**,**d**) *Hoyenella* sp. (samples TKV4.1 and TKV4.2, respectively). (**e**) *Glomospirella* sp. (sample TKV4.1). (**f**) Slightly curved, thin-shelled bivalve (?) (sample TKV4.1). (**g**) Goethitized pyrite aggregates scattered in aphanocrystalline to fine-crystalline dolomite matrix (sample TKV4.1). (**h**) Pore-filling Fe-calcite (indicated by pink to turquoise color) with polymodal crystal size distribution (sample TKV4.1; stained thin section). (**i**) Dull red to nonluminescent aphanocrystalline to fine-crystalline matrix dolomite with concentrically zoned blocky calcite cement (sample TKV4.2). CL = cathodoluminescence image, PPL = plane-polarized light.

4. Discussion

4.1. Reconstruction of the Depositional Environment

The micropetrographic analysis of the Anisian carbonate sequences from the Galşa, Măderat, and Valea cea Mică sections reveals a suite of microfacies characteristic of a shallow-marine carbonate depositional system, ranging from subtidal lagoons to peritidal (intertidal–supratidal) zones. These depositional patterns are consistent with broad sedimentological trends observed in the Western Tethyan realm during the Anisian, where extensive carbonate shelves developed (see [4,34–36]).

In the Galşa section, the identification of microbial boundstones (stromatolites) with perfectly preserved microbial textures is of primary significance for environmental reconstruction. These rocks exhibit undulating aphanocrystalline to fine-crystalline laminae interspersed with irregular fenestral pores. Recent studies have highlighted that such microbialites are not merely passive sediment traps but are actively induced by benthic microbial communities, often dominated by cyanobacteria and sulfate-reducing bacteria [37,38].

The fenestral fabrics observed are diagnostic of tidal flats where sediment is periodically exposed to the atmosphere, leading to desiccation and gas entrapment within the cohesive microbial mats ([39] and references therein). The fenestral voids are lined by fine- to medium-crystalline dolomite, indicating early cementation that prevented pore collapse. The preservation of these delicate fabrics in the fine-crystalline dolomite suggests that the microbial extracellular polymeric substances (EPSs) likely played a crucial role in organomineralization, serving as a template for early carbonate precipitation and protecting the texture from later diagenetic obliteration [37,40]. Recent works further highlight that the complex interplay between depositional conditions and multiphase diagenesis fundamentally controls the preservation and pore network evolution in microbial carbonate systems [41,42].

The biotic assemblage further constrains the paleoenvironment from a well-circulated lagoon (Galşa) to a restricted-to-semi-restricted lagoon/tidal flat setting within the photic zone (Măderat, Valea cea Mică). The abundance of dasycladalean algae, specifically *Teutloporella peniculiformis*, *Physoporella pauciforata undulata*, and *Physoporella pauciforata pauciforata* found in the Galşa section, indicates clear, shallow, and oligotrophic marine waters, as these algae are sensitive indicators of light penetration and salinity stability [43]. However, the co-occurrence of glomospirid foraminifers (*Glomospira articulosa*, *Glomospira gordialis*, *Glomospirella* sp.) and *Hoyenella sinensis* in the Măderat and Valea cea Mică sections points to intervals of environmental stress. In the context of Triassic Tethyan shelves, the dominance of these specific foraminiferal taxa is frequently associated with restricted, hypersaline, or oxygen-depleted back-reef lagoons where more stenohaline organisms could not thrive [44]. This aligns with studies on Triassic platform crises and global environmental perturbations [45], which suggest that fluctuating redox conditions and restricted circulation were common precursors to local ecosystem turnovers [46–48]. The presence of rip-up clasts and grainstones within these restricted facies reflects episodic high-energy events, such as tempestites generated via storms, which temporarily breached the morphological barriers and reworked the microbial mats [39].

4.2. Diagenetic Evolution

Although reconstruction of a detailed diagenetic history based on fabric-selective geochemical analyses is beyond the scope of this study, the micropetrographic observations presented above alone indicate that the studied successions record complex, multiphase diagenetic processes. A tentative paragenetic sequence is presented in Figure 9.

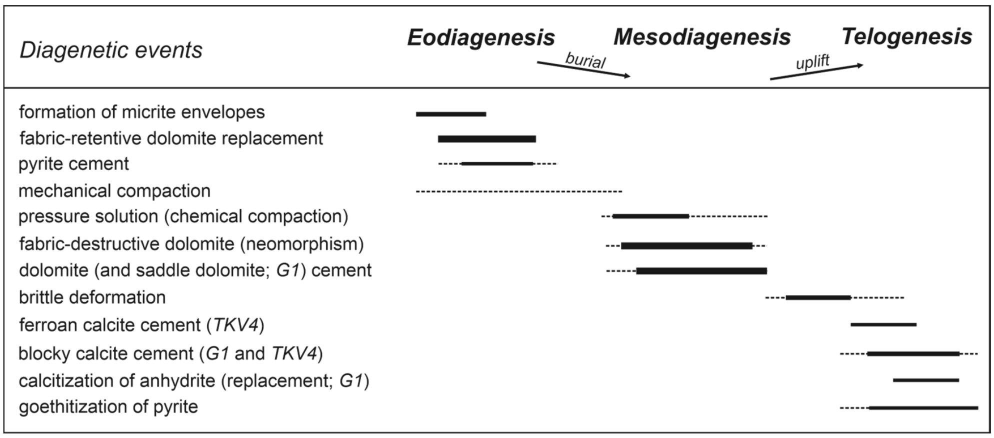

Figure 9. Preliminary paragenetic sequence of the Bulz Dolomite in the studied successions. Thick lines represent dominant features, thin lines indicate minor features, and dashed lines indicate uncertain temporal extent. The notations *G1* and *TKV4* are used for diagenetic events that, based on current data, are not ubiquitous throughout the entire study area of the Bulz Dolomite but are limited to the G1 and/or TKV4 sampling sites, respectively (see Figures 5–8).

4.2.1. Eodiagenesis

The earliest diagenetic modification involved the formation of micrite envelopes around bioclasts, a process attributed to microbial endolithic boring (micritization) on the seafloor, which outlined the original grains. The most critical early event, however, was the formation of fabric-retentive dolomite. The fine-crystalline nature of this dolomite, which preserves the intricate details of grains such as dasycladalean algae and stromatolites, suggests it formed prior to significant compaction, likely from fluids directly derived from coeval seawater. Recent models of "organogenic dolomitization" propose that the degradation of microbial EPSs in shallow burial environments releases magnesium and overcomes the kinetic barriers to dolomite precipitation at low temperatures [49–51]. This mechanism explains the preferential early diagenetic dolomitization of the studied sections. Additionally, the ubiquitous pyrite cement is most likely a product of early diagenetic sulfate reduction driven by seawater-derived pore fluids [39]. Furthermore, the localized presence of relic anhydrite partly replaced by late calcite indicates that the dolomitizing fluids were likely evaporitic brines, which are capable of driving pervasive dolomitization in arid, restricted platform settings (see [52] and references therein). Recent studies confirm that the association of dolomite with evaporite relics is a strong indicator of reflux dolomitization in restricted carbonate shelves [47,53–56]. Specifically, the calcitization of anhydrite suggests an interaction between the original evaporitic precipitates and later diagenetic fluids [57,58] (Figure 9).

4.2.2. Mesodiagenesis

As the carbonate shelf subsided, the sediments entered the realm of burial diagenesis. A second, more pervasive phase of dolomitization is represented by the fabric-destructive, coarse-crystalline dolomite with nonplanar-a to planar-s textures identified in the Galşa and Măderat sections. According to thermodynamic constraints, nonplanar textures generally develop at elevated temperatures (>50 °C), implying a burial origin where critical roughening temperatures were exceeded [59]. This recrystallization phase (neomorphism) likely obliterated the primary sedimentary structures in the Măderat section, leaving only "ghosts" of the original grains [60]. Additionally, the impact of increasing overburden pressure is evidenced by chemical compaction features, such as dissolution seams and microstylolites marked by insoluble brownish goethitic material.

The definitive evidence for deep burial or hydrothermal influence is the widespread occurrence of saddle dolomite cement filling vugs and fractures. These crystals exhibit characteristic curved faces, undulose extinction, and occasionally deformation twinning. Crystallographic studies have shown that the "saddle" distortion results from edge-nucleated growth and lattice warping due to rapid precipitation from highly supersaturated fluids [61,62]. The observed zonation in these cements, defined by alternating dark red–orange and bright red–orange CL bands, records fluctuating redox conditions (Mn/Fe ratios) in the burial fluids [63,64]. The dull to nonluminescent character of the matrix dolomite suggests it stabilized in a reducing, Fe-rich burial environment that quenched the luminescence. While often termed "hydrothermal," recent reviews clarify that saddle dolomite can form either from true hydrothermal fluids or from deep, hot basinal brines circulating along faults [57,65,66]. This represents a widespread phenomenon in multiphase dolomitized carbonate sequences, where late-stage hydrothermal or burial fluids overprint early fabric-retentive phases and occlude secondary porosity [67–69] (Figure 9). Regarding the timing, according to Garaguly et al. [20], the reservoir rocks from SE Hungary were affected by leaching from hydrothermal fluids during the Late Cretaceous thrusting.

4.2.3. Telogenesis

The final evolutionary stage is dominated by brittle deformation and fracture-controlled cementation. In the Valea cea Mică section, the lithology is described as a crackle breccia (sensu Woodcock and Mort [33]), where clasts are only slightly rotated and separated by hairline cracks. This texture is widely attributed to hydraulic fracturing near fault zones [70–72]. A fracture- and vug-filling ferroan calcite exhibiting turquoise to pink staining is specific to this locality, indicating precipitation under reducing conditions during the initial phase of the uplift [73]. As a general feature of the studied sections, a final generation of blocky calcite cement occluded the network of hairline cracks and vugs. The widespread goethitization of pyrite crystals and the replacement of late-stage cements suggest a final exposure to oxidizing meteoric waters. This likely occurred during the exhumation and uplift of the region (i.e., telogenesis), where meteoric fluids flushed through the fracture network, altering the earlier burial assemblages [74–76] (Figure 9). The above-reported multistage paragenesis mirrors the complex evolution of the Tethyan passive margins (see [77] and references therein).

4.3. Biostratigraphy

The biostratigraphic evaluation of the studied carbonate sequences in the Galşa, Măderat, and Valea cea Mică sections relies on the micropaleontological analysis of calcareous algae and benthic foraminiferal assemblages.

In the Galşa section, the fabric-retentive dolomite preserves a rich association of dasycladalean algae, which serves as the primary tool for high-resolution biostratigraphy in shallow-marine carbonates [43]. The identified assemblage includes *Teutloporella peniculiformis* Ott, *Physoporella pauciforata undulata* Bystrický, and *Physoporella pauciforata pauciforata* Bystrický. *Physoporella pauciforata* is a widely recognized index fossil for the Anisian stage in the Tethyan realm, with *P. pauciforata undulata* specifically characterizing the Pelsonian to lower Illyrian substages [78]. *Teutloporella peniculiformis* frequently co-occurs in the Anisian platform margin and lagoonal facies, supporting this stratigraphic assignment [39,79].

The biostratigraphy of the Măderat and Valea cea Mică sections is constrained by benthic foraminiferal associations dominated by glomospirids. The key taxon identified in both locations is *Hoyenella sinensis* (Ho). This miliolid foraminifer (formerly assigned to *Glomospirella shengi*) is a cosmopolitan marker species for the Anisian, particularly the Pelsonian substage, in the Tethyan domain [80]. While *Hoyenella sinensis* can range into the Ladinian, its high abundance in monospecific or low-diversity assemblages is typical of restricted Anisian lagoons [44]. At Măderat, *Hoyenella sinensis* occurs alongside *Glomospira articulosa* Plummer and *Glomospira gordialis* (Jones et Parker). *Glomospira gordialis* is a long-ranging Triassic taxon but is stratigraphically significant when found in association with *Hoyenella sinensis* in determining Middle Triassic platform interior environments [80,81]. Based on the presence of diagnostic taxa, all three studied sections are biostratigraphically correlated with the Anisian (Pelsonian–Illyrian) carbonate platforms in the western Tethys [78] and the Germanic Basin [82].

4.4. Regional Correlation

The biostratigraphic and lithological signatures of the Bulz Dolomite Formation (Apuseni Mountains, Romania) demonstrate compelling affinities with coeval Anisian carbonate sequences across the Carpathian–Pannonian realm. A diagnostic suite of Middle Triassic fossil assemblages strongly supports the existence of a unified, expansive shallow marine carbonate system extending across the Tisza Megaunit. Furthermore, examining these Anisian sequences alongside other Central European Triassic carbonate platforms, such as the thoroughly dolomitized Muschelkalk formations of the Germanic Basin [83], reveals similar complex geochemical and diagenetic evolutionary pathways across the broader region. In the Bulz Dolomite, dasycladalean algae, particularly *Teutloporella peniculiformis* and *Physoporella pauciforata*, serve as primary biostratigraphic markers [12,84]. These taxa align with the microflora of the Szeged Dolomite Formation in Hungary, which additionally hosts *Oligoporella* sp. and *Diplopora hexaster* (Table 1).

Table 1. Comparative list of fossils published from the Szeged Dolomite and Bulz Dolomite Formations [12,19,24,25,84] as well as those described in the current study (indicated by asterisk).

Szeged Dolomite Formation	Bulz Dolomite Formation
Algae	
Oligoporella sp. (Dasycladaleae)	*Teutloporella peniculiformis* Ott (Dasycladaleae) *
Diplopora hexaster Pia (Dasycladaleae)	*Physoporella pauciforata undulata* Bystrický (Dasycladaleae) *
Physoporella pauciforata undulata Pia (Dasycladaleae)	*Physoporella pauciforata pauciforata* Bystrický (Dasycladaleae) *
Fragments of algal colonies	Fragments of algal colonies
Foraminifers	
Trochammina almtalensis Koehn-Zaninetti	*Hoyenella sinensis* (Ho) *
Hoyenella sinensis (Ho)	*Hoyenella* sp. *
Glomospira tenuifistula Ho	*Glomospira articulosa* Plummer *
Glomospira densa Pantic	*Glomospira gordialis* (Jones et Parker) *
Glomospira regularis Lipina	*Glomospira* sp. *
Glomospira sp.	cf. *Glomospirella* sp. *
Glomospirella shengi Ho	cf. *Ammodiscus* sp. *
Glomospirella cf. *facilis* Ho	
Glomospirella sp.	
Ammodiscus sp.	
Endothyranella wirtzi Koehn-Zaninetti	
Meandrospira dinarica Kochansky-Devidé et Pantic	
Pilammina densa Pantic	
Flatschkofelia anisica Rettori et al.	
Earlandia sp.	
Others	
Ostracod shells	Ostracod shells *
Bivalve shells (Megalodontidae)	*Costatoria costata* (Zenker) (Bivalve)
Gastropod embryo shell	*Lyriomyophoria elegans* (Dunker) (Bivalve)
Echinoderm fragments	Bivalve shells *
	Gastropod shell
	Dadocrinus (Crinoidea)
	Echinoderm fragments *

The floral correlation is further corroborated by benthic foraminiferal assemblages—notably *Hoyenella sinensis* and *Glomospira* species—which appear in both the Bulz and Szeged formations, reflecting a widespread, shallow-marine biotope [25]. The Anisian age is constrained by macrofaunal evidence as well, including bivalves (*Costatoria costata*, *Lyriomyophoria elegans*) and *Dadocrinus* crinoids, establishing a direct chronostratigraphic link

https://doi.org/10.3390/geosciences16050170

with the wider Tethyan realm, namely with the Transdanubian Range [4]. Together, these biotic markers indicate that despite minor provincial variations in taxonomic abundance, the region shared a contiguous shallow-marine ecosystem.

Based on published data, the deposition of the Szeged Dolomite extends into the Ladinian [19,27]. However, there is no documented evidence that the stratigraphic range of the Bulz Dolomite is similar; only Anisian age data are available, and it appears that the drowning of the shallow-marine carbonate shelf in the Apuseni Mountains already occurred during the Late Anisian [3,4]. Naturally, this does not rule out the possibility that Ladinian biostratigraphic data might be recovered in the future from Bulz Dolomite sections that have not yet been studied in detail.

Reconstruction of the original depositional environments reveals that the studied Anisian dolomites predominantly formed in shallow-marine, peritidal to subtidal settings along the Neotethyan passive margin. Under prevailing arid climatic conditions, this paleogeographic position favored intense evaporation and subsequent reflux-driven dolomitization. While the overarching depositional system was uniform, local facies variations highlight distinct sub-environments. The Bulz Dolomite is characterized by stromatolitic laminites, peloidal wackestones, and pervasive microbial fabrics, pointing to sedimentation within restricted lagoons subjected to intermittent evaporitic conditions. Periodic subaerial exposure in this region is evidenced by rip-up clasts and fenestral porosity. Similar peritidal dynamics are recorded in the Szeged Basin, where microbial laminites and evaporite pseudomorphs are prevalent [20,26], transitioning locally into deeper subtidal zones dominated by crinoid-bivalve packstones. Parallel peritidal conditions, marked by tepee structures, quartz pseudomorphs after gypsum, and well-developed microbial mats, have also been documented in other areas of the Tisza Megaunit, namely in the Mecsek and Villány Hills [22,85], further underscoring the regional extent of this evaporitic, shallow-water carbonate sedimentary system.

The diagenetic history of the region exhibits a complex evolution, initially driven by early marine processes and subsequently overprinted by local geological factors. The first stage, early dolomitization, is characterized by fabric-retentive dolomite uniformly present across all studied regions, indicating the penecontemporaneous reflux of Mg-rich brines. In the Bulz Dolomite, this early phase successfully preserved primary microbial fabrics and delicate bioclasts, such as foraminifers. As a result of subsidence, burial recrystallization initiated a fabric-destructive phase. Driven by progressive burial diagenesis, late-stage saddle dolomite cements and microstylolites formed within the Bulz Dolomite, recording intermediate burial deformation and subsequent deep-burial fluid migration. Comparable diagenetic signatures are observed regionally; the nonplanar and saddle dolomite cements of both the Szeged Dolomite [20] and the Anisian Kán Dolomite in the Mecsek Mountains [85] crystallized from deep-burial-related hydrothermal fluids. Ultimately, each studied Anisian dolomite formation exhibits late-stage meteoric calcite cementation—likely triggered by Paleogene–Miocene uplift—which partially occluded the remaining primary and secondary porosity.

5. Conclusions

This study provides the first detailed micropetrographic and biostratigraphic documentation of the Anisian Bulz Dolomite Formation (Apuseni Mountains) in the international literature. By integrating microfacies analysis with preliminary diagenetic and paleontological data, the research yields the following key findings:

1. Depositional environment: The Bulz Dolomite developed in a shallow-marine carbonate shelf interior, comprising restricted subtidal lagoons and peritidal (intertidal–supratidal) zones. The excellent preservation of microbial boundstones (stromatolites)

with fenestral fabrics, combined with restricted algal and foraminiferal assemblages, points to an arid paleoclimate characterized by intense evaporation and periodic subaerial exposure.

2. Biostratigraphy: A diagnostic fossil assemblage of dasycladalean algae (e.g., *Teutloporella peniculiformis*, *Physoporella pauciforata*) and benthic foraminifers (notably *Hoyenella sinensis* and *Glomospira* spp.) firmly constrains the formation to the Anisian (Pelsonian–Illyrian) stage.
3. Multiphase diagenetic evolution: The dolomitization of the sequence followed a complex pathway. It initiated with early, fabric-retentive reflux dolomitization driven by hypersaline, Mg-rich brines derived from coeval seawater. Subsequent progressive burial led to fabric-destructive recrystallization and the precipitation of saddle dolomite cements from hot, deep-basinal or hydrothermal fluids. A final telogenetic stage was marked by brittle deformation (crackle breccia formation) and the influx of meteoric fluids, resulting in late-stage calcite cementation.
4. Regional correlation and paleogeography: This research resolves previous stratigraphic ambiguities by linking the Bulz Dolomite with the heavily explored, hydrocarbon-bearing Szeged Dolomite Formation in Hungary. The matching microfacies, biostratigraphic markers, and diagenetic pathways confirm the existence of an extended evaporitic carbonate shelf across the Tisza Megaunit along the Neotethyan passive margin during the Middle Triassic.

Author Contributions: Conceptualization, B.R. and A.V.; methodology, B.R. and A.V.; formal analysis, B.R. and A.V.; investigation, B.R., A.V., O.P. and A.S.K.; writing—original draft preparation, B.R. and A.V.; writing—review and editing, B.R., A.V., O.P., A.S.K. and E.P.-M.; visualization, B.R. and A.V.; funding acquisition, A.V. and E.P.-M. All authors have read and agreed to the published version of the manuscript.

Funding: The research was supported by the National Research, Development and Innovation Fund of Hungary (projects no. K 108375 and K 131690).

Data Availability Statement: The original contributions presented in this study are included in the article. Further inquiries can be directed to the corresponding author.

Acknowledgments: This study represents a collaborative effort by members of the "Terra Tempus" Paleoclimate and Paleoenvironment Research Group, University of Szeged. The authors are grateful to Attila Bencsik and Viktor Granyák for preparing the thin sections that form the basis of this research.

Conflicts of Interest: The authors declare no conflicts of interest.

References

1. Ianovici, V.; Borcoş, M.; Bleahu, M.; Patrulius, D.; Lupu, M.; Dimitrescu, R.; Savu, H. *Geologia Munților Apuseni*; Editura Academiei RSR: Bucharest, Romania, 1976. (In Romanian)
2. Bleahu, M.; Lupu, M.; Patrulius, D.; Bordea, S.; Stefan, A.; Panin, S. *The Structure of the Apuseni Mts. Guide to Excursion B3*; 12th CBGA Congress, Bucureşti; Guidbook Series 23; Institute of Geology and Geophysics: Bucharest, Romania, 1981; pp. 1–107.
3. Bleahu, M.; Mantea, G.H.; Haas, J.; Kovács, S.; Péró, C.; Bordea, S.; Panin, S.; Bérczi-Makk, A.; Ştefănescu, M.; Konrád, G.; et al. Triassic facies types, evolution, paleogeographic relations of the Tisza Megaunit. *Acta Geol. Hung.* **1994**, *37*, 187–234.
4. Haas, J.; Péró, C. Mesozoic evolution of the Tisza Mega-unit. *Int. J. Earth Sci.* **2004**, *93*, 297–313. [CrossRef]
5. Vozárová, A.; Ebner, F.; Kovács, S.; Kräutner, H.G.; Szederkényi, T.; Krstić, B.; Sremac, J.; Aljinovič, D.; Novak, M.; Skaberne, D. Late Variscan (Carboniferous to Permian) environments in the Circum Pannonian Region. *Geol. Carpathica* **2009**, *60*, 71–104. [CrossRef]
6. Kovács, S.; Sudar, M.; Grădinaru, E.; Gawlick, H.-J.; Karamata, S.; Haas, J.; Péró, C.; Gaetani, M.; Mello, J.; Polák, M.; et al. Triassic Evolution of the Tectonostratigraphic Units of the Circum-Pannonian Region. *Jahrb. Der Geol. Bundesanst. Wien.* **2011**, *151*, 199–280.

7. Schmid, S.M.; Fügenschuh, B.; Kounov, A.; Maţenco, L.; Nievergelt, P.; Oberhänsli, R.; Pleuger, J.; Schefer, S.; Schuster, R.; Tomljenović, B.; et al. Tectonic units of the Alpine collision zone between Eastern Alps and western Turkey. *Gondwana Res.* **2020**, *78*, 308–374. [CrossRef]
8. Papiu, C.V.; Ghenea, C. *Notă Explicativă. Harta Geologică a Republicii Socialiste România, Scara 1:200 000, 16. Arad*; Institute of Geology and Geophysics: Bucharest, Romania, 1966; 25p. (In Romanian)
9. Bleahu, M.; Borcoş, M.; Savu, H. *Notă Explicativă. Harta Geologică a Republicii Socialiste România, Scara 1:200 000, 17. Brad*; Institute of Geology and Geophysics: Bucharest, Romania, 1968; 61p. (In Romanian)
10. Patrulius, D.; Lupu, M.; Borcoş, M. *Notă Explicativă. Harta Geologică a Republicii Socialiste România, Scara 1:200 000, 09. Şimleul Silvaniei*; Institute of Geology and Geophysics: Bucharest, Romania, 1968; 46p. (In Romanian)
11. Patrulius, D.; Bleahu, M.; Popescu, I.; Bordea, S. *The Triassic Formations of the Apuseni Mountains and of East Carpathian Bend*; Guidebook to Excursion of the 2nd Triassic Colloquium, CBGA; Guidbook Series 8; Institute of Geology and Geophysics: Bucharest, Romania, 1971; pp. 1–86.
12. Patrulius, D.; Bleahu, M.; Antonescu, E.; Baltreş, A.; Bordea, S.; Bordea, J.; Gheorghian, D.; Iordan, M.; Mirăuţă, E.; Panin, Ş.; et al. *The Triassic Formations of the Bihor Autochthon and Codru Nappe-System (Apuseni Mountains); Guidebook to Excursion of the 3rd Triassic Colloquium, CBGA*; Institute of Geology and Geophysics: Bucharest, Romania, 1979; 31p.
13. Vozár, J.; Ebner, F.; Vozárová, A.; Haas, J.; Kovács, S.; Sudar, M.; Bielik, M.; Péró, C. (Eds.) *Variscan and Alpine Terranes of the Circum-Pannonian Region*; Slovak Academy of Sciences, Geological Institute: Bratislava, Slovakia, 2010; 233p.
14. Lazăr, I.; Sandy, M.R.; Forel, M.B.; Grădinaru, E.; Peckmann, J.; Grădinaru, M. Late Triassic brachiopod *Halorella* assemblages from paleokarst cavities near Vașcău, Apuseni Mountains, Romania. In Proceedings of the Abstract Volume of the 11th Romanian Symposium of Palaeontology, Bucharest, Romania, 27–28 September 2017; pp. 71–72.
15. Lazăr, I.; Schlagintweit, F.; Grădinaru, E. *Halorina cryptica* nov. ichnogen., nov. ichnosp., mass-occurrence of Upper Triassic crustacean microcoprolites from neptunian dikes and sills cutting the Dachstein-type carbonate platform and their paleoenvironmental significance (Northern Apuseni Mountains, Romania). *Geobios* **2020**, *61*, 31–39. [CrossRef]
16. Mircescu, C.V.; Tămaș, T.; Bucur, I.I.; Săsăran, E.; Ungureanu, R.; Mircescu, V.; Mircescu, E.; Oprişa, A. Upper Triassic–Lower Jurassic continental carbonates from the Apuseni Mountains, Romania: Facies, lithology and paleoenvironments. *Facies* **2021**, *67*, 15. [CrossRef]
17. Kounov, A.; Schmid, S.M. Fission-track constraints on the thermal and tectonic evolution of the Apuseni Mountains (Romania). *Int. J. Earth Sci.* **2013**, *102*, 207–233. [CrossRef]
18. Varga, A.; Pozsár, A.; Zajzon, N.; Topa, B.; Benkó, Z.; Pál-Molnár, E.; Raucsik, B. Effects of Metasomatism on Granite-Related Mineral Systems: A Boron-Rich Open Greisen System in the Highiş Granitoids (Apuseni Mountains, Romania). *Minerals* **2023**, *13*, 1083. [CrossRef]
19. Bérczíné Makk, A. Mesozoic formation types of the Great Hungarian Plain. *Acta Geol. Hung.* **1986**, *29*, 261–282.
20. Garaguly, I.; Varga, A.; Raucsik, B.; Schubert, F.; Czuppon, G.; Frei, R. Pervasive early diagenetic dolomitization, subsequent hydrothermal alteration, and late stage hydrocarbon accumulation in a Middle Triassic carbonate sequence (Szeged Basin, SE Hungary). *Mar. Pet. Geol.* **2018**, *98*, 270–290. [CrossRef]
21. Machel, H.G. Concepts and models of dolomitization: A critical reappraisal. In *The Geometry and Petrogenesis of Dolomite Hydrocarbon Reservoirs*; Braithwaite, C.J.R., Rizzi, G., Darke, G., Eds.; Geological Society, London, Special Publications: London, UK, 2004; Volume 235, pp. 7–63. [CrossRef]
22. Lukoczki, G.; Haas, J.; Gregg, J.M.; Machel, H.G.; Kele, S.; John, C.M. Early dolomitization and partial burial recrystallization: A case study of Middle Triassic peritidal dolomites in the Villány Hills (SW Hungary) using petrography, carbon, oxygen, strontium and clumped isotope data. *Int. J. Earth Sci.* **2020**, *109*, 1051–1070. [CrossRef]
23. Haas, J.; Budai, T.; Győri, O.; Czuppon, G. Development and dolomitization of Anisian isolated carbonate platforms in the Transdanubian Range, Hungary. *Cent. Eur. Geol.* **2022**, *65*, 14–25. [CrossRef]
24. Bérczíné Makk, A. Types of Mesozoic sequence in the Great Hungarian Plain. *Általános Földtani Szle.* **1985**, *21*, 3–47. (In Hungarian)
25. Horváth, A. Szedimentáció- és Diagenezis Vizsgálatok D-Alföldi Szénhidrogénkutató Fúrások Anizuszi Dolomit (Szegedi Terület) és Nagyharsányi Mészkő (Bácskai Terület) Képződményein. Doctoral Thesis, Eötvös Loránd University, Budapest, Hungary, 1990. (In Hungarian)
26. Garaguly, I.; Raucsik, B.; Varga, A.; Schubert, F. Középső-triász dolomitok képződésének története és töréses deformációja a Szegedi-medence területén. *Földt. Közlöny* **2017**, *147*, 39–60, (In Hungarian with English abstract). [CrossRef]
27. Szurominé Korecz, A.; Garaguly, I.; Szente, I.; Varga, A.; Raucsik, B. „Oasis in the desert"—A particularly rich fossil assemblage from the fossil-poor Szeged Dolomite Formation, Üllés (Szeged Basin, Hungary). *Földt. Közlöny* **2018**, *148*, 119–124, (In Hungarian with English abstract). [CrossRef]
28. Săndulescu, M. *Geotectonics of Romania*; Editura Tehnică: Bucharest, Romania, 1984; 336p. (In Romanian)
29. Dickson, J.A.D. Carbonate identification and genesis as revealed by staining. *J. Sediment. Res.* **1966**, *36*, 491–505. [CrossRef]
30. Folk, R.L. Practical petrographic classification of limestones. *AAPG Bull.* **1959**, *43*, 1–38. [CrossRef]

31. Dunham, R.J. Classification of carbonate rocks according to their depositional texture. In *Classification of Carbonate Rocks*; Ham, W.E., Ed.; AAPG Memoir: Tulsa, OK, USA, 1962; Volume 1, pp. 108–121.
32. Embry, A.F.; Klovan, J.E. Absolute water depth limits of Late Devonian paleoecological zones. *Geol. Rundsch.* **1972**, *61*, 672–686. [CrossRef]
33. Woodcock, N.H.; Mort, K. Classification of fault breccias and related fault rocks. *Geol. Mag.* **2008**, *145*, 435–440. [CrossRef]
34. Haas, J.; Budai, T.; Győri, O.; Kele, S. Similarities and differences in the dolomitization history of two coeval Middle Triassic carbonate platforms, Balaton Highland, Hungary. *Facies* **2014**, *60*, 581–602. [CrossRef]
35. Gawlick, H.J.; Lein, R.; Bucur, I.I. Precursor extension to final Neo-Tethys break-up: Flooding events and their significance for the correlation of shallow-water and deep-marine organisms (Anisian, Eastern Alps, Austria). *Int. J. Earth Sci.* **2021**, *110*, 419–446. [CrossRef]
36. Karádi, V.; Budai, T.; Haas, J.; Vörös, A.; Piros, O.; Dunkl, I.; Tóth, E. Change from shallow to deep-water environment on an isolated carbonate platform in the Middle Triassic of the Transdanubian Range (Hungary). *Palaeogeogr. Palaeoclimatol. Palaeoecol.* **2022**, *587*, 110793. [CrossRef]
37. Perri, E.; Tucker, M.E. Bacterial fossils and microbial dolomite in Triassic stromatolites. *Geology* **2007**, *35*, 207–210. [CrossRef]
38. Moonpa, K.; Udchachon, M.; Jainanta, J.; Kanthata, S. Microbial carbonates of Upper Triassic Doi Long Formation, Lampang Group: A study of new outcrop localities in northern Lampang, central north Thailand. *Diversity* **2025**, *17*, 299. [CrossRef]
39. Flügel, E. *Microfacies of Carbonate Rocks: Analysis, Interpretation and Application*, 2nd ed.; Springer: Berlin/Heidelberg, Germany, 2010; 984p. [CrossRef]
40. Suarez-Gonzalez, P.; Benito, M.I.; Quijada, I.E.; Mas, R.; Campos-Soto, S. 'Trapping and binding': A review of the factors controlling the development of fossil agglutinated microbialites and their distribution in space and time. *Earth-Sci. Rev.* **2019**, *194*, 182–215. [CrossRef]
41. Ullah, I.; Jamil, M.; Ur Rahim, H.; Khan, I.; Ali, A.; Muzammil, M.; Abbas, W.; Umar, M.; Shah, F.; Usman, M. Impact of Diagenesis on Microbial Carbonate Reservoirs in the Upper Indus Basin, NW Himalayas. *Minerals* **2026**, *16*, 111. [CrossRef]
42. Wang, Y.; Liu, H.; Jiang, W.; Shi, K.; Liu, B.; Zheng, H. The impacts of sedimentary micro-textures and diagenesis on the pore structure of microbial dolomite in the Middle Triassic Leikoupo Formation, western Sichuan Basin, China. *Pet. Geosci.* **2026**, *32*, petgeo2025-050. [CrossRef]
43. Berger, S.; Kaever, M.J. *Dasycladales: An Illustrated Monograph of a Fascinating Algal Order*; Georg Thieme Verlag: Stuttgart, Germany, 1992; 192p, ISBN 978-3137743019.
44. Kaminski, M.A. The new and reinstated genera of agglutinated foraminifera published between 1986 and 1996. In *Proceedings of the Fifth International Workshop on Agglutinated Foraminifera*; Hart, M.B., Kaminski, M.A., Smart, C.W., Eds.; Grzybowski Foundation Special Publication: Kraków, Poland, 2000; Volume 7, pp. 185–219.
45. Dal Corso, J.; Mills, B.J.W.; Chu, D.; Newton, R.J.; Song, H. Background Earth system state amplified Carnian (Late Triassic) environmental changes. *Earth Planet. Sci. Lett.* **2022**, *578*, 117321. [CrossRef]
46. Stefani, M.; Furin, S.; Gianolla, P. The changing climate framework and depositional dynamics of Triassic carbonate platforms from the Dolomites. *Palaeogeogr. Palaeoclimatol. Palaeoecol.* **2010**, *290*, 43–57. [CrossRef]
47. Pérez-López, A.; Benedicto, C.; Ortí, F. Middle Triassic carbonates of Eastern Iberia (Western Tethyan Realm): A shallow platform model. *Sediment. Geol.* **2021**, *420*, 105904. [CrossRef]
48. Tóth, E.; Baranyi, V.; Karádi, V.; Jin, X.; Budai, T. Ostracod turnover during the Carnian Pluvial Episode (Late Triassic) in the Western Neotethys. *Palaeogeogr. Palaeoclimatol. Palaeoecol.* **2024**, *650*, 112379. [CrossRef]
49. Bontognali, T.R.R.; McKenzie, J.A.; Warthmann, R.J.; Vasconcelos, C. Microbially influenced formation of Mg-calcite and Ca-dolomite in the presence of exopolymeric substances produced by sulphate-reducing bacteria. *Terra Nova* **2014**, *26*, 72–77. [CrossRef]
50. Areias, C.; Barbosa, C.F.; Cruz, A.P.S.; McKenzie, J.A.; Ariztegui, D.; Eglinton, T.; Haghipour, N.; Vasconcelos, C.; Sánchez-Román, M. Organic matter diagenesis and precipitation of Mg-rich carbonate and dolomite in modern hypersaline lagoons linked to climate changes. *Geochim. Cosmochim. Acta* **2022**, *337*, 14–32. [CrossRef]
51. Meng, R.; Han, Z.; Nie, W.; Han, C.; Han, Y.; Tucker, M.E. Mineralization of bacterial cells during proto-dolomite precipitation mediated by the halophilic bacteria *Bacillus licheniformis*. *Chem. Geol.* **2026**, *701*, 123205. [CrossRef]
52. Warren, J.K. Dolomite: Occurrence, evolution and economically important associations. *Earth-Sci. Rev.* **2000**, *52*, 1–81. [CrossRef]
53. Laya, J.C.; Teoh, C.P.; Whitaker, F.; Manche, C.; Kaczmarek, S.; Tucker, M.; Gabellone, T.; Hasiuk, F. Dolomitization of a Miocene-Pliocene progradational carbonate platform by mesohaline brines: Re-examination of the reflux model on Bonaire Island. *Mar. Pet. Geol.* **2021**, *126*, 104895. [CrossRef]
54. Jones, G.D.; Xiao, Y. Dolomitization, anhydrite cementation, and porosity evolution in a reflux system: Insights from reactive transport models. *AAPG Bull.* **2005**, *89*, 577–601. [CrossRef]
55. Alqattan, M.; Budd, D.A. Dolomite and dolomitization of the Permian Khuff-C reservoir in Ghawar field, Saudi Arabia. *AAPG Bull.* **2017**, *101*, 1715–1745. [CrossRef]

56. Zhong, S.; Liu, Z.; Jin, Z.; Tian, H.; Istifanus, M.A.; George, S.C. The Development of Dolomite Within a Sequence Stratigraphic Framework: Cambrian Series 2 Changping Formation, Xiaweidian, China. *Minerals* **2024**, *14*, 1189. [CrossRef]
57. Kendall, A.C. Late diagenetic calcitization of anhydrite from the Mississippian of Saskatchewan, western Canada. *Sedimentology* **2001**, *48*, 29–55. [CrossRef]
58. Chen, P.; Fu, M.; Deng, H.; Xu, W.; Wu, D.; He, P.; Guo, H. The diagenetic alteration of the carbonate rocks from the Permian Qixia Formation as response to two periods of hydrothermal fluids charging in the central uplift of Sichuan Basin, SW China. *Minerals* **2021**, *11*, 1212. [CrossRef]
59. Sibley, D.F.; Gregg, J.M. Classification of dolomite rock textures. *J. Sediment. Petrol.* **1987**, *57*, 967–975. [CrossRef]
60. Ren, G.; Qin, Q.; Qin, Z.; Guo, Y.; Ye, Z. Effects of diagenesis on quality of deep dolomite reservoirs: A case study of the Upper Cambrian Xixiangchi Formation in the eastern Sichuan Basin, China. *Front. Earth Sci.* **2022**, *10*, 984463. [CrossRef]
61. Searl, A. Saddle dolomite: A new view of its nature and origin. *Mineral. Mag.* **1989**, *53*, 547–555. [CrossRef]
62. Machel, H.G.; Lonnee, J.S. Hydrothermal dolomite—A product of poor definition and imagination. *Sediment. Geol.* **2002**, *152*, 163–171. [CrossRef]
63. Machel, H.G. Application of cathodoluminescence to carbonate diagenesis. In *Cathodoluminescence in Geosciences*; Pagel, M., Barbin, V., Blanc, P., Ohnenstetter, D., Eds.; Springer: Berlin/Heidelberg, Germany, 2000; pp. 271–301. [CrossRef]
64. Kyle, J.R.; Quintero, T.R.; Ukar, E.; Miller, N.R.; Elliott, S.J.; Colbert, M. Dolomite cement microstratigraphy: A record of brine evolution and ore precipitation mechanisms, upper Knox Group, Tennessee and Kentucky, USA. *Geology* **2023**, *51*, 392–396. [CrossRef]
65. Davies, G.R.; Smith, L.B. Structurally controlled hydrothermal dolomite reservoir facies: An overview. *AAPG Bull.* **2006**, *90*, 1641–1690. [CrossRef]
66. Mansurbeg, H.; Alsuwaidi, M.; Morad, D.; Morad, S.; Tiepolo, M.; Shahrokhi, S.; Al-Aasm, I.S.; Koyi, H. Disconformity-controlled hydrothermal dolomitization and cementation during basin evolution: Upper Triassic carbonates, UAE. *Geology* **2024**, *52*, 486–491. [CrossRef]
67. Hao, R.; Pan, L.; Mu, N.; Li, X.; Fu, X.; Xiong, S.; Liu, S.; Zheng, J.; She, M.; Munnecke, A. Multi-Phase Dolomitization in the Jurassic Paleo-Oil Reservoir Zone, Qiangtang Basin (SW China): Implications for Reservoir Development. *Minerals* **2024**, *14*, 908. [CrossRef]
68. Liu, Z.; Zhang, H.; Hu, Y. Sedimentary facies and reservoir evolution of the Cretaceous Alamein Formation, Alamein Basin, northern Western Desert, Egypt. *J. Afr. Earth Sci.* **2026**, *236*, 106020. [CrossRef]
69. Li, S.; Gao, J.; Yang, T.; Li, T.; Liu, T.; Hao, Y.; He, Z.; Liu, E. Source and U-Pb Chronology of Diagenetic Fluids in the Permian Maokou Formation Dolomite Reservoir, Eastern Sichuan Basin, China. *Minerals* **2024**, *14*, 803. [CrossRef]
70. Li, Z.; Eaton, D.; Davidsen, J. Short-term forecasting of M_{max} during hydraulic fracturing. *Sci. Rep.* **2022**, *12*, 12509. [CrossRef]
71. Rysak, B.; Gale, J.; Laubach, S.; Ferrill, D. Mechanisms for the generation of complex fracture networks: Observations from Slant core, analog models, and outcrop. *Front. Earth Sci.* **2022**, *10*, 848012. [CrossRef]
72. Chan, L.S.; Alvarez, W.; Geiser, P.; Tavarnelli, E. Fluid-assisted brecciation of Lower Cretaceous Maiolica limestone in the Umbria-Marche Apennines: Hydrodynamical implications. In *From the Guajira Desert to the Apennines, and from Mediterranean Microplates to the Mexican Killer Asteroid: Honoring the Career of Walter Alvarez*; Koeberl, C., Claeys, P., Montanari, A., Eds.; Geological Society of America Special Papers: Boulder, CO, USA, 2022; Volume 557, pp. 99–114. [CrossRef]
73. Richter, D.K.; Füchtbauer, H. Ferroan calcite replacement indicates former magnesian calcite skeletons. *Sedimentology* **1978**, *25*, 843–860. [CrossRef]
74. Holail, H. Coordinated petrography-isotopic-chemical investigation of meteoric calcite cement (Jurassic-Pleistocene), Egypt. *Carbonates Evaporites* **1992**, *7*, 48–55. [CrossRef]
75. Hashim, M.S.; Kaczmarek, S.E. Rhombic calcite microcrystals as a textural proxy for meteoric diagenesis. *Sci. Rep.* **2022**, *12*, 213. [CrossRef]
76. Gasparrini, M.; Mangenot, X.; Bonifacie, M.; Deschamps, P.; Ceriani, A. Cooling and Exhumation History of the Paris Basin Southeastern Margin Revealed by Δ_{47}/U–Pb Carbonate Thermochronology. *Terra Nova* **2025**, *37*, 421–430. [CrossRef]
77. Amidon, W.H.; Kylander-Clark, A.R.C.; Barr, M.N.; Graf, S.F.I.; West, D.P. Pace of passive margin tectonism revealed by U-Pb dating of fracture-filling calcite. *Nat. Commun.* **2022**, *13*, 1953. [CrossRef]
78. Piros, O. Anisian to Carnian carbonate platform facies and dasycladacean biostratigraphy of the Aggtelek Mts, Northeastern Hungary. *Acta Geol. Hung.* **2002**, *45*, 119–151. [CrossRef]
79. Ott, E. Die Kalkalgen-Chronologie der alpinen Mitteltrias in Angleichung an die Ammoniten-Chronologie. *Neues Jahrb. Geol. Paläontol. Abh.* **1972**, *141*, 81–115, (in German with English abstract). [CrossRef]
80. Maurer, F.; Rettori, R. Middle Triassic Foraminifera from the Seceda core (Dolomites, Northern Italy). *Riv. Ital.Paleontol. Stratigr.* **2002**, *108*, 391–398. [CrossRef]
81. Del Piero, N.; Rigaud, S.; Peybernes, C.; Forel, M.B.; Farley, N.; Martini, R. Upper Triassic Carbonate Records: Insights from the Most Complete Panthalassan Platform (Lime Peak, Yukon, Canada). *Geosciences* **2022**, *12*, 292. [CrossRef]

82. Bucur, I.I.; Michał, M. Dasycladalean green algae and associated foraminifers in Middle Triassic (lower and middle Muschelkalk) carbonates of the south-eastern Germanic basin (upper Silesia, Poland). *Ann. Soc. Geol. Pol.* **2020**, *90*, 391–407. [CrossRef]
83. Stanienda-Pilecki, K.J.; Jendruś, R. Geochemical and Mineralogical Characteristics of Triassic Dolomites from Upper Silesia, Poland. *Minerals* **2024**, *14*, 371. [CrossRef]
84. Bércziné Makk, A.; Konrád, G.; Rálischné Felgenhauer, E.; Török, Á. Tiszai Egység. In *Magyarország Geológiája, Triász*; Haas, J., Ed.; Eötvös Kiadó: Budapest, Hungary, 2004; pp. 303–354. (In Hungarian)
85. Lukoczki, G.; Haas, J.; Gregg, J.M.; Machel, H.G.; Kele, S.; John, C.M. Multi-phase dolomitization and recrystallization of Middle Triassic shallow marine-peritidal carbonates from the Mecsek Mts. (SW Hungary), as inferred from petrography, carbon, oxygen, strontium and clumped isotope data. *Mar. Pet. Geol.* **2019**, *101*, 440–458. [CrossRef]